Chemical and Pharmaceutical Bulletin Advance Publication by J-STAGE
DOI:10.1248/cpb.c23-00410

Advance Publication
September 14, 2023

A fluorescence biosensor for tyrosinase activity analysis based on silicon-doped carbon quantum dots

Qiang Chen[a], Lili Zheng[b,^], Xiaoqin Deng[b], Menghan Zhang[b], Wendi Han[c,*], Zhengjun Huang[b], Chenfang Miao[b,d,*], Shaohuang Weng[b]

a Department of Andrology & Sexual Medicine, the First Affiliated Hospital of Fujian Medical University, Fuzhou, 350005, China

b Department of Pharmaceutical Analysis, School of Pharmacy, Fujian Medical University, Fuzhou 350122, China

c Department of Pharmacy, the First Affiliated Hospital of Fujian Medical University, Fuzhou, 350005, China

d Department of Pharmacy, The 900th Hospital of Joint Logistics Team of the PLA, Fuzhou General Clinical Medical College of Fujian Medical University, Fuzhou 350025, China

* Correspondence: monday0796@163.com (C. Miao); colour2124@163.com (W. Han)

^: Current address: Minxi Vocational & Technical College, Longyan, 364021, China

Abstract

Tyrosinase (TYR) plays a pivotal role in the biosynthesis of melanin, and its activity level holds critical implications for vitiligo, melanoma cancer, and food nutritional value. The sensitive determination of TYR activity is of great significance for both fundamental research and clinical investigations. In this work, we successfully synthesized silicon-doped carbon quantum dots (Si-CQDs) through a one-pot hydrothermal method with trans-aconitic acid as carbon source and N-[3-(Trimethoxysilyl)propyl]ethylenediamine as the dopant, exhibiting remarkable fluorescence quantum yield (QY) and photostability. Correspondingly, Si-CQDs were used as a probe to construct a sensitive, rapid, and user-friendly fluorescence method for TYR detection. The method relied on the oxidation of isoprenaline (ISO) by TYR, where Si-CQDs were employed as a highly efficient probe. The testing mechanism was the internal filtering effect (IFE) observed between Si-CQDs and the oxidative system of ISO and TYR. Under the optimized conditions, the fluorescence strategy exhibited a detection range of 0.05-2.0 U/mL for TYR with a limit of detection (LOD) of 0.041 U/mL. Furthermore, we successful demonstrated the accurate determination of TYR levels in human serum, showcasing the promising potential of this method in various practical scenarios.

Keywords: Silicon doped carbon quantum dots; Fluorescence strategy; Isoprenaline; Tyrosinase; Internal filtering effect

1. Introduction

Tyrosinase (TYR) is a copper-containing polyphenol oxidase with wide distribution in animals, plants, and microorganisms. Its enzymatic function involves hydroxylating phenolic substrates into catechol derivatives and subsequently oxidizing them into o-quinone products (participating in the formation of melanin) in the presence of molecular oxygen [1,2]. Among them, melanin plays a critical role in fighting against oxidative stress, controlling skin colour, and safeguarding cellular DNA against harmful ultraviolet radiation [3,4]. Notably, dysregulation of TYR levels in humans has been associated with the development of various diseases, including Parkinson's syndrome, vitiligo, and melanoma [5-7]. As a result, TYR serves as a significant biomarker in clinical diagnosis of melanoma cancer [8]. Moreover, TYR also exerts a substantial influence on the nutritional value of food [9]. Therefore, achieving accurate and real-time monitoring of TYR activity becomes indispensable for clinical diagnosis, disease treatment, and nutritional analysis of food.

To date, several analytical strategies have been reported for detecting TYR, including electrochemistry [10,11], high-performance liquid chromatography [12], electrophoresis [13], colorimetry [14], and surface-enhanced Raman spectroscopy [15]. However, these methods are usually accompanied by one or more limitations of poor repeatability, time-consuming, complex operating procedures, and the need for specific professional instruments [16,17]. Thus, there is a pressing need to develop simpler and more accurate TYR sensors for in situ measurements. Fluorescence analysis has aroused great interest in biosensors due to its low cost, simplicity of operation, real-time performance, and controllable sample pretreatment [18]. Although some TYR fluorescence assays have been developed in recent years utilizing molecular probes [17,19], inorganic semiconductor quantum dots [4] and gold/silver nanoclusters [20], these probes have potential shortcomings, such as tedious and time-consuming synthesis process, high cytotoxicity and poor stability. Therefore, the search of a new fluorescent nanomaterial probe with enhanced properties to construct a fluorescence sensing platform for TYR remains an important research focus and has strong support for the realization of effective determination of TYR.

Carbon quantum dots (CQDs) are a class of zero-dimensional carbon nanomaterials characterized by their ultra-fine, dispersed, and quasi-spherical nanoparticle structure, with sizes below 10 nm. The unique properties of CQDs, including simple preparation, excellent water solubility, and ease of surface functionalization, stable and tunable luminescence properties, make them highly promising candidates for fluorescence sensing [21-23]. CQDs have been successfully used to detect various biomolecules including trypsin [24], hyaluronidase [25], and alkaline phosphatase [26,27]. While, most of the fluorescent CQDs used for TYR activity detection still encounter the lack of low fluorescence quantum yield (QY) and poor sensitivity, which hinder the prospects of biological applications [28-30]. It is known that doping of heteroatoms (such as N, Si, S, B) is one of the most effective methods to improve and adjust the photophysical and chemical properties of CQDs [31-33]. Introducing heteroatom leads to significant changes in the electronic distribution and related electronic energy levels of CQDs, thereby affecting the energy band gap and luminous efficiency, and ultimately realizing the tunability of luminous properties [34]. Additionally, diverse functional groups containing heteroatoms play a crucial role in modulating the properties of CQDs and achieving broad applications in biosensing [35-38].

Silicon, an element of the same main group as carbon, as a dopant into CQDs, can significantly modulate the properties of CQDs and provide more active sites, and thereby resulting in enhanced properties [39-41]. Trans-aconitic acid and N-[3-(Trimethoxysilyl)propyl]ethylenediamine (DAMO) have been applied as the raw molecule for the bottom-up preparations of carbon quantum dots with a certain application, respectively [42,43]. Herein, we successfully obtained silicon-doped carbon quantum dots (Si-CQDs) with high fluorescence QY (69%), and excellent photostability by hydrothermal method using trans-aconitic acid as the carbon source and DAMO as the dopant. Leveraging the enzymatic catalytic properties of TYR on the oxidation of isoprenaline (ISO), we constructed a fluorescent signal-off strategy for TYR detection using Si-CQDs as probe and ISO as substrate. This method showed excellent analytical performance, including wide linear range, low detection limit, and

anti-interference ability, and was expected to realize rapid in situ determination of TYR. This work heralds the design and development of a fluorescent probe with excellent luminescent properties that is expected to improve detection performance for the methodological support of the diagnosis of clinical diseases.

2 Experimental sections

2.1 Materials and Instrumentation

Tyrosinase (TYR), dopamine hydrochloride (DA), trypsin (Try), alkaline phosphatase (ALP), and glucose oxidase (GOD) were purchased from Sigma-Aldrich (Shanghai, China). Isoprenaline (ISO), dopamine (DA), levodopa (L-DA), adrenaline (AD), and norepinephrine (NE), trans-aconitic acid, N-[3-(Trimethoxysilyl)propyl] ethylenediamine (DAMO), glycine (Gly), glucose (Glu), bovine serum albumin (BSA), ROX (6-carboxy-X-rhodamine), and FAM (6-carboxyfluorescein) were supplied by Aladdin Reagent Co., Ltd. (Shanghai, China). No evolutionary processing was operated for any of the reagents used in this study.

The fluorescence spectrum was recorded on a fluorescence spectrophotometer (Cary Eclipse, Agilent Technologies, USA), while the UV-visible absorption spectrum was scanned by a UV-visible spectrophotometer (UV-2450, Shimadzu Corporation, Japan). For the fluorescence lifetime decay curve, a FS5 fluorescence spectrometer (Edinburgh Instruments, Britain) was utilized. Transmission electron microscopy (TEM) was operated on JEM-2100F (JEOL, Japan) at 200 kV for morphological evaluation. X-ray Diffractometer (XRD) of Si-CQDs was carried out on D8 Advance (Bruker, Germany). X-ray photoelectron spectrometer (ESCALAB 250XI, Thermo Fisher Scientific, USA) and Fourier transform infrared spectroscopy (NICOLET iS50, Thermo Fisher Scientific, USA) were employed to analyse the molecular structure of Si-CQDs.

2.2 Synthesis of Si-CQDs

The silicon-doped CQDs (Si-CQDs) with high quantum yield were prepared by a one-pot hydrothermal method. Specifically, a mixture of trans-aconitic acid (0.1741 g, 50 mM) and N-[3-(Trimethoxysilyl)propyl]ethylenediamine (DAMO) (2 mL, 462.3 mM) were dissolved in 18 mL of ultrapure water in a conical flask under the nitrogen

protection. The mixture was thoroughly stirred for 20 min and then transferred to a 50 mL polytetrafluoroethylene reactor for further reaction at 200 ℃ for 24 h. The resulting solution was filtered through a 0.22 μm microporous membrane and purified using a dialysis bag (MWCO: 500-1000 Da) for 48 h. After freeze-drying, a stock solution of Si-CQDs was prepared and stored at 4 ℃.

2.3 Determination of the relative fluorescence QY of Si-CQDs

The relative fluorescence QY of Si-CQDs ($QY_{Si\text{-}CQDs}$) was determined with quinine sulfate (QS) as a reference. Initially, the absorptions of Si-CQDs in an aqueous solution and QS dissolved in 0.1 M H_2SO_4 (QY_{QS}=54.6%) were determined at a wavelength of 370 nm (A<0.06), respectively. Subsequently, the emission spectra of the above solutions were further measured at 370 nm excitation. Finally, the curve slope ratio of Si-CQDs to QS ($\frac{K_{Si\text{-}CQDs}}{K_{QS}}$) was obtained by taking absorbance as the X axis and the integral area of fluorescence spectrum as the Y axis. Then, the $QY_{Si\text{-}CQDs}$ was achieved from Formula 1.

$$\frac{QY_{Si\text{-}CQDs}}{QY_{QS}} = \frac{K_{Si\text{-}CQDs}}{K_{QS}} \left(\frac{\eta_{Si\text{-}CQDs}}{\eta_{QS}} \right)^2$$

Formula 1

$QY_{Si\text{-}CQDs}$ and QY_{QS}, $K_{Si\text{-}CQDs}$ and K_{QS}, $\eta_{Si\text{-}CQDs}$, and η_{QS} were the QY, curve slope and solvent refractive index of Si-CQDs and QS, respectively ($\eta_{Si\text{-}CQDs}$=1.33, η_{QS}=1.33).

2.4 The morphology characterization of Si-CQDs

The morphology of Si-CQDs was investigated using TEM. The dispersion of Si-CQDs was diluted with water/ethanol as a dispersant to achieve a uniform and well-dispersed solution. The solution was dropped into the ultra-thin copper mesh after 15 minutes of ultrasound, and further recorded the morphology and structure of the Si-CQDs with TEM.

2.5 Determination of TYR based on the mixture of Si-CQDs and ISO

A mixture solution containing 1 mM ISO and Si-CQDs (25 μg/mL) was reacted with different concentrations of TYR (0-20 U/mL) in 200 μL pH 7.4 phosphate-buffered saline (PBS) respectively. The incubation was carried out at 37 ℃ for 2 h. Subsequently,

the fluorescence emission spectra of the different Si-CQDs+ISO+TYR with variable TYR contents were recorded in the range of 380-650 nm with exciting at 370 nm. The mixture of Si-CQDs with ISO or TYR was defined as Si-CQDs+ISO or Si-CQDs+TYR. The solution of Si-CQDs+ISO for TYR detection was defined as Si-CQDs+ISO+TYR. F_0 and F are the fluorescence intensities of Si-CQDs+ISO at 450 nm in the absence and presence of TYR, respectively.

2.6 Selectivity of TYR detection

To assess the selectivity of this method, a series of common and related interferents, like enzymes and proteins, were selected for evaluation. The interferents (GOD, Gly, Glu, Trypsin, BSA, and ALP) were added individually to a mixture containing Si-CQDs (25 μg/mL) and 1 mM ISO in 200 μL of pH 7.4 PBS, in the presence of 5 U/mL TYR. The mixtures were then allowed to react at 37 ℃ for 2 h. The fluorescence spectra were recorded and compared in the range of 380-650 nm with 370 nm excitation.

2.7 Detecting TYR in human serum samples

Human serum from healthy donors was obtained and applied to evaluate the feasibility of this assay for TYR detection in biological samples. Specifically, the different concentrations of TYR (1.25, 1.75, 1.75, 2.00 U/mL) were added to the mixed solution of Si-CQDs (25 μg/mL) and 1 mM ISO in 200 μL pH 7.4 PBS containing 1% serum, respectively. After keeping the condition at 37 ℃ for 2 h, the fluorescence spectra were recorded in the range of 380-650 nm with 370 nm excitation.

3 Result and discussion

3.1 Optical properties and structural characterization of Si-CQDs

The optical properties, morphology, and molecular structure of Si-CQDs were characterized. As shown in Fig. 1A, the fluorescence intensities of Si-CQDs initially increased and then decreased under excitation at 320-390 nm, exhibiting the excitation-independent luminescence behavior. The maximum excitation and emission wavelengths of Si-CQDs were 370 nm and 450 nm, respectively. The UV-vis absorption spectrum of Si-CQDs (Fig. 1B) showed two characteristic absorption peaks at 240 nm and 380 nm, attributing to the π-π^* electronic transition of C=C and n-π^* electronic transition of C=O, respectively [44,45]. Remarkably, the relative quantum yield of Si-CQDs (E_x=370 nm, $QY_{Si\text{-}CQDs}$) was evaluated to be 69%, using quinine sulfate (E_x=350 nm, QY_{QS}=54.6%) as reference (Fig. 1C). Notably, this QY value surpassed that of

many previously reported carbon quantum dots [28,40,41,46,47]. The TEM result (Fig. 1D) suggested that Si-CQDs were monodisperse spherical particles with dispersion and uniformity. The particle size of Si-CQDs ranged from 1.0 nm to 4.0 nm, with an average diameter of 3.12 nm (upper left inset in Fig. 1D). Furthermore, the XRD pattern of Si-CQDs (lower right inset in Fig. 1D) showed a broad diffraction peak centered at approximately 21°, indicating the nearly amorphous nature of Si-CQDs [48,49]. The FTIR and XPS were applied to evaluate the molecular functional groups and elemental composition of Si-CQDs. As shown in FTIR spectrum (Fig. 1E), the absorption peaks at 3420 cm^{-1} were ascribed to the stretching vibration of O-H/N-H. The typical absorption bands at 1658 cm^{-1} and 1316 cm^{-1} can be considered as the stretching vibration of the amide bond (O=C-N), resulting from the coupling between the amino group of DAMO and the carboxyl group of trans-aconitic acid. Additionally, the peaks at 1110 cm^{-1}/1020 cm^{-1} and 928 cm^{-1} were assigned to the stretching vibration of Si-O-Si and Si-O-H respectively, implying the successful doping of Si. The presence of amino and Si-O groups facilitated enhanced surface functionalizations and the conjugated carbon structure of Si-CQDs, thereby contributing to their improved fluorescent properties [50,51]. Furthermore, the elemental composition of Si-CQDs was analyzed by XPS (Fig. 1F). The full-wavelength XPS spectrum showed the five typical peaks attributed to C1s, N1s, O1s, Si2s, and Si2p at 285.08 eV, 399.08 eV, 530.8 eV, 152.08 eV, and 101.08 eV, respectively [39]. The corresponding atomic contents were calculated to be 47.32% (C), 12.85% (N), 25.04% (O) and 14.79% (Si). The relatively high contents of N and Si may promote an enhancement in the quantum yield of Si-CQDs [52]. In conclusion, the comprehensive characterization of Si-CQDs revealed their enhanced luminescent properties, regular and uniform particle size distribution, and the presence of abundant surface oxygen-containing functional groups.

3.2 Optical stability of Si-CQDs

The fluorescence stability of Si-CQDs was assessed by investigating their fluorescence signal responses under various conditions. As illustrated in Fig. S1A, Si-CQDs exhibited relative fluorescence stability within a pH range of pH 4-12, with only a slight increase in fluorescence intensity observed under strongly alkaline conditions

(pH 11-12), indicating their stable pH property. Additionally, Si-CQDs exhibited stable fluorescence intensity over a broad temperature range from 5 to 90 ℃ (Fig. S1B) and across solutions with varying degrees of salt concentrations, from low to high (Fig. S1C). Furthermore, the photobleaching resistance of Si-CQDs was meticulously evaluated and compared with that of the organic dyes of FAM and ROX when subjected to exposure under a 300 W xenon lamp for 240 minutes. The fluorescent intensities of FAM and ROX significantly decreased, while the fluorescent intensities of Si-CQD remained stable compared to its original intensity (Fig. S1D). Moreover, the fluorescence intensities of Si-CQDs remained stable when stored at 4 ℃ for extended periods of 30-50 days (Fig. S1E), indicating outstanding photobleaching resistance and long-term luminescence stability. The successful doping of silicon is believed to have significantly contributed to the enhanced optical properties of Si-CQDs, enabling them to display superior fluorescence stability across various environmental conditions.

3.3 The detecting feasibility of TYR using Si-CQDs+ISO

In general, TYR functions as a catalyst for the oxidation of phenolic substrates, leading to o-quinones formation. This process may affect the fluorescence signal of carbon fluorescent nanomaterials like Si-CQDs, as used in this work. The feasibility studies were conducted on a system where the oxidation of ISO catalyzed by TYR interacted with Si-CQDs. As shown in Fig. 2A, TYR and ISO had a minor effect on the fluorescence intensity of Si-CQDs. While significant changes occurred in the fluorescence intensity of Si-CQDs when TYR was added to the mixture of Si-CQDs and ISO (Si-CQDs+ISO). It was concluded that the feasibility of using the fluorescence signal-off strategy, with ISO as the substrate and Si-CQDs as the probe, to determine TYR activity. Additionally, TYR, as a copper-containing polyphenol oxidase, can oxidize ISO analogs (including dopamine (DA), levodopa (L-DA), adrenaline (AD), and norepinephrine (NE)) to produce o-quinone through enzymatic catalysis. As shown in Fig 2B, the action of TYR and DA or other ISO analogs all result in fluorescence quenching of Si-CQDs. Among them, TYR's enzymatic catalysis using ISO as substrate had the greatest impact on the fluorescence quenching efficiency (QE, $((F_0-F)/F_0)$) of Si-CQDs (Fig 2B). Therefore, ISO was selected as the appropriate catalytic substrate

of TYR for the construction of the fluorescence strategy to detect TYR using Si-CQDs as a probe.

3.4 The detecting mechanism of TYR in the Si-CQDs+ISO+TYR system

The mechanism underlying the quenching of Si-CQDs with ISO as the substrate by TYR was thoroughly investigated. As shown in Fig. 3A, the fluorescence lifetimes of Si-CQDs were found to be 13.85 ns and 13.76 ns in the absence and presence of ISO and TYR, respectively. This observation indicated the absence of dynamic quenching effect (DQE) of Si-CQDs in Si-CQDs+ISO+TYR system. Subsequently, the UV-vis absorption spectrum (Fig. 3B) revealed important insights into the reaction solution of ISO oxidized by TYR (TYR+ISO). TYR+ISO showed a new UV absorption peak at 306 nm and a broad absorption peak centered at 450 nm compared to TYR and ISO alone. Importantly, the positions of these two peaks remained unchanged upon the addition of Si-CQDs, signifying complete overlapping of the UV absorption peaks between TYR+ISO and Si-CQDs+ISO+TYR. This observation indicated that there was no static quenching effect (SQE) in the Si-CQDs+ISO+TYR system. Generally, the sufficient overlapping of the absorption band of an absorber (quenching agent) with the excitation and/or emission bands of a fluorophore can result in an inner filter effect (IFE) [53]. It was worth noting that the broad absorption peak centered at 450 nm of o-quinones produced by the oxidation of ISO by TYR coincided with the fluorescence emission spectrum of Si-CQDs (Fig. 3C), suggesting a possible IFE between Si-CQDs and TYR+ISO [47]. The E correction was further performed according to the parameters of the quartz cuvette geometry (inset in Fig. 3D) and Formula S1 [54]. As shown in Fig. 3D and Table S1, the $E_{observed}$ value significantly differed from that of $E_{corrected}$ with the addition of different concentrations of TYR ($E_{observed}$ and $E_{corrected}$ were calculated by Formula S2). It was evident that the TYR detection strategy, utilizing Si-CQDs as the probe and ISO as the substrate, relied on the IFE between Si-CQDs and ISO+TYR [54]. The overlapping between the absorption band of o-quinones and the emission spectrum of Si-CQDs sensitively regulated the fluorescence signal of Si-CQDs based on IFE, thus enabling efficient detection of TYR activity.

3.5 Optimization of experimental conditions

The experimental conditions, including pH, reaction time, temperature, and ISO concentration, were systematically optimized to ensure the accuracy and reliability of the measurement. The pH of the buffer was a critical factor affecting TYR's enzymatic activity. As strong acids and bases significantly affect the activity of TYR, the fluorescence QE ($(F_0-F)/F_0$) was evaluated in the Si-CQDs+ISO+TYR system in the pH range of 5.0-8.5. As shown in Fig. S2A, the QE of Si-CQDs gradually increased as the pH increased from 5.0 to 7.4. However, it started to decrease when the pH was further increased from 7.4 to 8.5. Therefore, pH 7.4 was chosen as the optimal condition for measuring TYR activity in this work. Furthermore, considering the practical application and physiological conditions of TYR, the reaction temperature was investigated at 25 ℃, 30 ℃, and 37 ℃, and the reaction time was varied from 10 to 150 minutes. The QE of ISO+TYR to Si-CQDs was found to increase with the rise in temperature (25-37 ℃, Fig. S2B) and reaction time (10-150 minutes, Fig. S2C), reaching its maximum at 37 ℃ and 120 minutes, respectively. Therefore, the optimal reaction temperature and time were selected as 37 ℃ and 120 minutes with the simulated physiological environment of pH 7.4. On the other hand, the effect of ISO concentration on the testing system was investigated. As shown in Fig. S2D, with increasing ISO concentrations, the QE of the testing system gradually increased, plateauing after the addition of 1 mM ISO. Thus, 1 mM ISO was chosen as the appropriate concentration for detecting TYR activity.

3.6 Analytical performance of TYR

Under the optimized conditions, the variable fluorescence intensities of Si-CQDs+ISO modulated by TYR were investigated. It was found that the fluorescence intensities gradually decreased with increasing TYR concentrations (Fig. 4A). The ΔF ($\Delta F=F_0-F$) gradually enhanced and reached the plateau (Fig. 4B), and there was a good linear relationship between ΔF and C_{TYR} (the concentration of TYR) in the range of 0.05-2.0 U/mL. The linear equation of $Y=140.297C_{TYR}+46.1892$ ($R^2=0.99231$) (inset in Fig. 4B) was obtained for ΔF and C_{TYR}, and the limit of detection (LOD) was calculated to be 0.041 U/mL (S/N=3, n=8). The impact of common interfering

substances, such as enzymes and proteins (GOD, Gly, Glu, Trypsin, BSA, and ALP), on the fluorescence intensities of Si-CQDs+ISO+TYR, were investigated. As shown in Fig. 4C, TYR could selectively catalyze the oxidation of ISO and quench the fluorescence signal of Si-CQDs. Meanwhile, the QE of Si-CQDs+ISO+TYR remained unchanged when these common interfering substances were added, indicating that the signal-off strategy based on Si-CQDs+ISO had high selectivity for TYR detection.

This method was evaluated for the determination of TYR in human serum, as shown in Table S2. The spiked recovery of TYR was 96.2%-98.1% with the RSD in the range of 1.25%-2.51%. The results demonstrated that this method had good accuracy in the determination of TYR, and had credibility and practicality in practical analysis. Compared with the existing methods (Table S3), this study established a fluorescence method with Si-CQDs as a probe and ISO as a substrate to detect TYR with high sensitivity and a wide linear range. In addition, this method had the characteristics of simple operation and no need of expensive instruments, which could realize the simple but effective monitoring of TYR.

4 Conclusion

In summary, our study successfully synthesized Si-CQDs using trans-aconitic acid and N-[3-(Trimethoxysilyl)propyl]ethylene-diamine as precursors through a one-pot hydrothermal method. The resulting Si-CQDs exhibited remarkable excitation-independent luminescence characteristics, along with high fluorescence QY and photostability. The doping of Si was found to be a key factor in modulating the photophysical and chemical properties of Si-CQDs. Accordingly, based on the catalytic oxidation of ISO by TYR and further quenching the fluorescence signal of Si-CQDs through IFE, we successfully constructed a fluorescence sensing strategy for TYR detection, with Si-CQDs serving as the sensitive probe. This study provides valuable insight for the development of fluorescent carbon quantum dots with controllable photophysical and chemical properties, offering promising avenues to enhance the sensitivity and accuracy of detecting target substances, such as TYR. Moreover, this work offers promising implications for expanding the field of biological application of

carbon quantum dots based on improving optical properties and clinical considerations about the diagnosis.

Acknowledgement

The authors gratefully acknowledge financial support from the National Science Foundation of Fujian Province (Nos. 2021J01714, 2021J01694, 2022J01493), and the Youth independent innovation project incubation project of the 900th Hospital of Joint Logistics Team of the PLA (No. 2022QC09).

Author Contributions

Qiang Chen, Lili Zheng, Wendi Han: Methodology, Data curation, Formal analysis, Visualization, Writing-original draft, Writing - review & editing. Xiaoqin Deng and Menghan Zhang: Methodology, Data curation, Formal analysis, Visualization. Zhengjun Huang: Formal analysis, Chenfang Miao and Shaohuang Weng: Conceptualization, Formal analysis, Project administration, Writing-original draft, Writing - review & editing.

Conflict of interest

The authors declare no conflict of interest.

Supplementary materials

This article contains supplementary materials.

Reference

1) Guo N., You X., Wu Y., Du D., Zhang L., Shang Q., Liu W., Anal. Chem., **92**, 5780-5786 (2020).
2) Pan L., Huang K., Min G., Li X., Shao J., Ma F., Kong L., Zou M., Meng G., Chen W., Sens. Actuators. B. Chem., **358**, 131474 (2022).
3) Ma X., Gao W., Halawa M. I., Lan Y., Li J., Xu G., Sens. Actuators. B. Chem., **280**, 41-45 (2019).
4) Li S., Zhao R., Ma M., Fu G., Mu S., Han T., Liu X., Zhang H., Sens. Actuators. B. Chem., **370**, 132438 (2022).
5) Lin T. E., Bondarenko A., Lesch A., Pick H., Cortés-Salazar F., Girault H. H., Angew. Chem. Int. Edi., **55**, 3813-3816 (2016).
6) Zhu X., Hu J., Zhao Z., Sun M., Chi X., Wang X., Gao J., Small, **11**, 862-870 (2015).
7) Cao J., Gong J., Fu N., Microchem. J., **173**, 107007 (2022).
8) Dai Q., Wang X., Liu C, Feng Z., Ge B., Ma X., Zhang Z., Yu J., Wang X., Huang F., Anal. Chim. Acta, **1169**, 338605 (2021).
9) Taherkhani N., Hekmat A., Piri H., Haghbeen K., J. Food Biochem., **46**, 14279 (2022).
10) Zeng H., Zhou S., Xie L., Zhang X., Zeng J., Yan M., Liang Q., Liu T., Liang K., Zhang L., Anal. Chem., **94**, 2589-2596 (2021).
11) Wang L., Gan Z. F., Guo D., Xia H. L., Patrice F. T., Hafez M. E., Li D. W., Anal. Chem., **91**, 6507-6513 (2019).
12) Li W., Zhang Y., Shi S., Yang G., Liu Z., Wang J., Kang W., Food Chem. Toxicol., **133**, 110754 (2019).
13) Nellaiappan K., Vinayagam A., Stain Technol., **61**, 269-272 (1986).
14) Deng H. H., Lin X. L., He S. B., Wu G. W., Wu W. H., Yang Y., Lin Z., Peng H. P., Xia X. H., Chen W., Microchim. Acta, **186**, 1-7 (2019).
15) Li M., Lu D., You R., Shen H., Zhu L., Lin Q., Lu Y., J. Phys. Chem. C, **126**, 12651-12659 (2022).
16) Zhang W. H., Ma W., Long Y. T., Anal. Chem., **88**, 5131-5136 (2016).
17) Qu Y., Zhan Q., Du S., Ding Y., Fang B., Du W., Wu Q., Yu H., Li L., Huang W., J. Pharm. Anal., **10**, 414-425 (2020).
18) Guo Y., Zhao W., Coordin. Chem. Rev., **387**, 249-261 (2019).
19) Wu X., Li L., Shi W., Gong Q., Ma H., Angew. Chem. Int. Edi., **55**, 14728-14732 (2016).
20) Ao H., Qian Z., Zhu Y., Zhao M., Tang C., Huang Y., Feng H., Wang A., Biosens. Bioelectron., **86**, 542-547 (2016).
21) Liu M. L., Chen B. B., Li C. M., Huang C. Z., Green Chem., **21**, 449-471 (2019).
22) Wang W., Cheng L., Liu W., Sci. China Chem., **57**, 522-539 (2014).
23) Jorns M., Pappas D., Nanomaterials, **11**, 1448 (2021).
24) Yin C., Chen L., Niu N., Anal. Bioanal. Chem., **413**, 5239-5249 (2021).
25) Yang W., Ni J., Luo F., Weng W., Wei Q., Lin Z., Chen G., Anal. Chem., **89**, 8384-8390 (2017).
26) Qian Z. S., Chai L. J., Huang Y. Y., Tang C., Shen J. J., Chen J. R., Feng H., Biosens. Bioelectron., **68**, 675-680 (2015).
27) Lv Y., Chen J., Zhou X., Su X., Anal. Bioanal. Chem., **414**, 7989-7998 (2022).
28) Luo T., Chen Y., Wang Y., Mater. Today Sustain., **19**, 100207 (2022).
29) Gu B., Chen D., Gao B., Liu Z., Wang Z., Wang T., Yang Y., Guo Q., Wang G., ChemistrySelect, **5**, 7155-7163 (2020).
30) Markovic Z. M., Labudova M., Danko M., Matijasevic D., Micusik M., Nadazdy V., Kovacova

M., Kleinova A., Spitalsky Z., Pavlovic V., ACS Sustain. Chem. Eng., **8**, 16327-16338 (2020).
31) Chang S., Chen B. B., Lv J., Fodjo E. K., Qian R. C., Li D. W., Microchim. Acta, **187**, 1-8 (2020).
32) Liu Q., Niu X., Zhang Y., Zhao Y., Xie K., Yang B., He Q., Lv S., Li L., Nanoscale, **12**, 13010-13016 (2020).
33) Lu L., Tu D., Liu Y., Zhou S., Zheng W., Chen X., Nano Res., **11**, 264-273 (2018).
34) Cheng R., Xiang Y., Guo R., Li L., Zou G., Fu C., Hou H., Ji X., Small, **17**, 2102091 (2021).
35) Kadian S., Sethi S. K., Manik G., Mater. Chem. Front., **5**, 627-658 (2021).
36) Hallaji Z., Bagheri Z., Oroujlo M., Nemati M., Tavassoli Z., Ranjbar B., Microchim. Acta, **189**, 190 (2022).
37) Iravani S., Varma R. S., Environ. Chem. Lett., **18**, 703-727 (2020).
38) Pandey S., Bodas D., Adv. Colloid Interfac., **278**, 102137 (2020).
39) Qian Z., Shan X., Chai L., Ma J., Chen J., Feng H., ACS Appl. Mater. Interfaces, **6**, 6797-6805 (2014).
40) M. Desai., H. Basu., S. Saha., R. Singhal., S. Kailasa., Opt. Mater., **96**: 109374 (2019).
41) Sun Z., Zhou W., Luo J., Fan J., Wu Z. C., Zhu H., Huang J., Zhang X., J. Colloid Interface Sci., **607**, 16-23 (2022).
42) Yi Z. H., Li X. M., Zhang H. Y., Ji X. L., Sun W., Yu Y. X., Liu Y. N., Huang J. X., Sarshar Z., Sain M., Talanta, **222**, 121663 (2021).
43) Gao L. P., Wang C. L., Xu S. H., Xia P. F., Liu F., Sun H. C., Wang Z. Y., Lu C. G., Cui Y. P., ACS Appl. Nano Mater., **5**, 7850-7857 (2022).
44) Shen X. B., Song B., Fang B., Yuan X., Li Y. Y., Wang S. Y., Ji S. J., He Y., Nano Res., **12**, 315-322 (2019).
45) Feng Y., Liu Y., Su C., Ji X., He Z., Sens. Actuators. B. Chem., **203**, 795-801 (2014).
46) Huang S., Li W., Zhou X., Xie M., Luo Q., Wen H., Luo Y., Xue W., Microchem. J., **159**, 105456 (2020).
47) Han W., Miao C., Zhang X., Lin Y., Hao X., Huang Z., Weng S., Lin X., Guo X., Huang J., Anal. Chim. Acta, **1179**, 338853 (2021).
48) Wu S., Li W., Zhou W., Zhan Y., Hu C., Zhuang J., Zhang H., Zhang X., Lei B., Liu Y., Adv. Opt. Mater., **6**, 1701150 (2018).
49) Das P., Ganguly S., Agarwal T., Maity P., Ghosh S., Choudhary S., Gangopadhyay S., Maiti TK., Dhara S., Banerjee S., Mater. Chem. Phys., **237**, 121860 (2019).
50) Ai L., Yang Y. S., Wang B. Y., Chang J. B., Tang Z. Y., Yang B., Lu S. Y., Sci. Bull., **66**, 839-856 (2021);
51) Kou X. L., Jiang S. C., Park S. J., Meng L. Y., Dalton Trans., **49**, 6915-6938 (2020).
52) Desai M. L., Basu H., Saha S., Singhal R. K., Kailasa S. K., Opt. Materi., **96**, 109374 (2019).
53) Wang J., Qiu F. X., Wu H. Y., Li X., Zhang T., Niu X. H., Yang D. Y., Pan J. M., Xu J. C., Spectrochim. Acta A, **179**, 163-170 (2017).
54) Liu J., Chen Y., Wang W., Feng J., Liang M., Ma S., Chen X., J. Agric. Food Chem., **64**, 371-380 (2016).

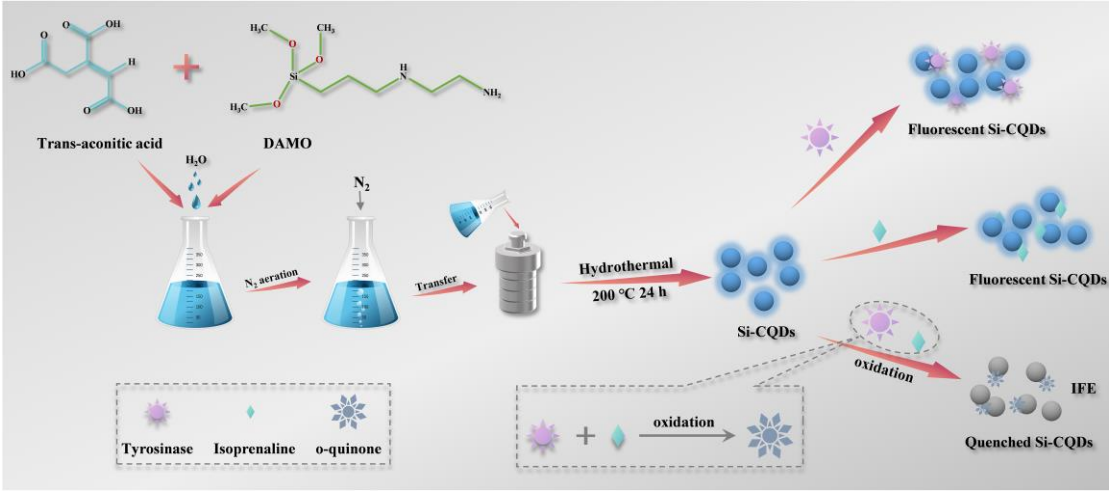

Chart 1 Schematic illustration of the preparation of the Si-CQDs and the application in TYR detection.

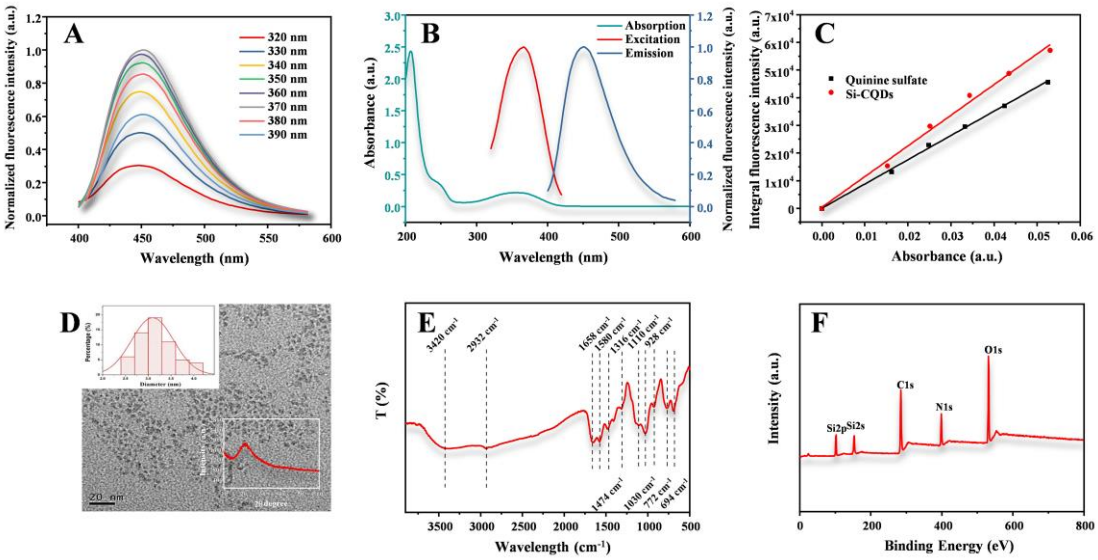

Fig. 1 (A) Fluorescence emission spectra of Si-CQDs at 320-390 nm excitation. (B) The UV-vis, and fluorescence excitation and emission spectra of Si-CQDs. (C) The relative QY of Si-CQDs with quinine sulfate as reference. The TEM image (size distribution chart (upper left) and XRD spectrum (lower right)) (D), FTIR spectrum (E), and XPS spectrum (F) of Si-CQDs.

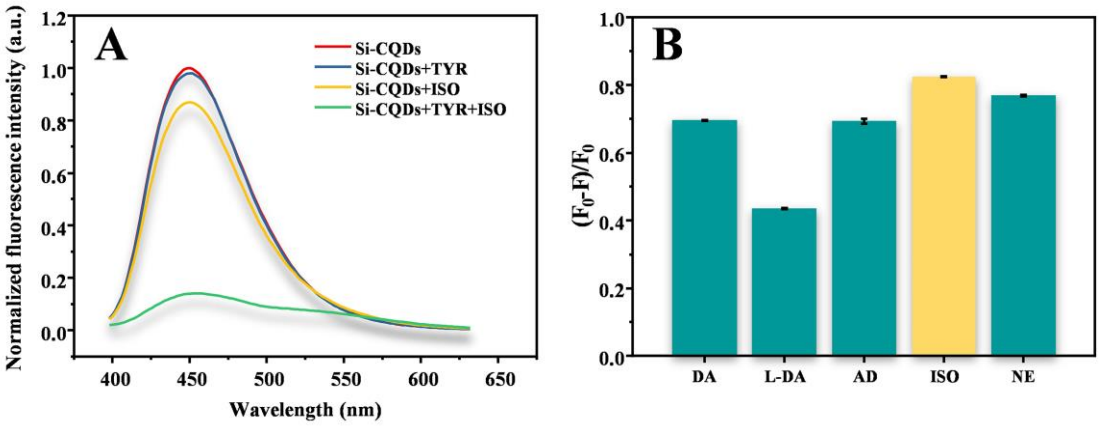

Fig. 2 (A) The normalized fluorescence emission spectra of Si-CQDs, Si-CQDs+TYR, Si-CQDs+ISO, and Si-CQDs+TYR+ISO. (B) The effects of DA, L-DA, AD, ISO, and NE on the $(F_0\text{-}F)/F_0$ of Si-CQDs+TYR. The concentrations of DA, L-DA, AD, ISO, and NE are 1 mM, respectively.

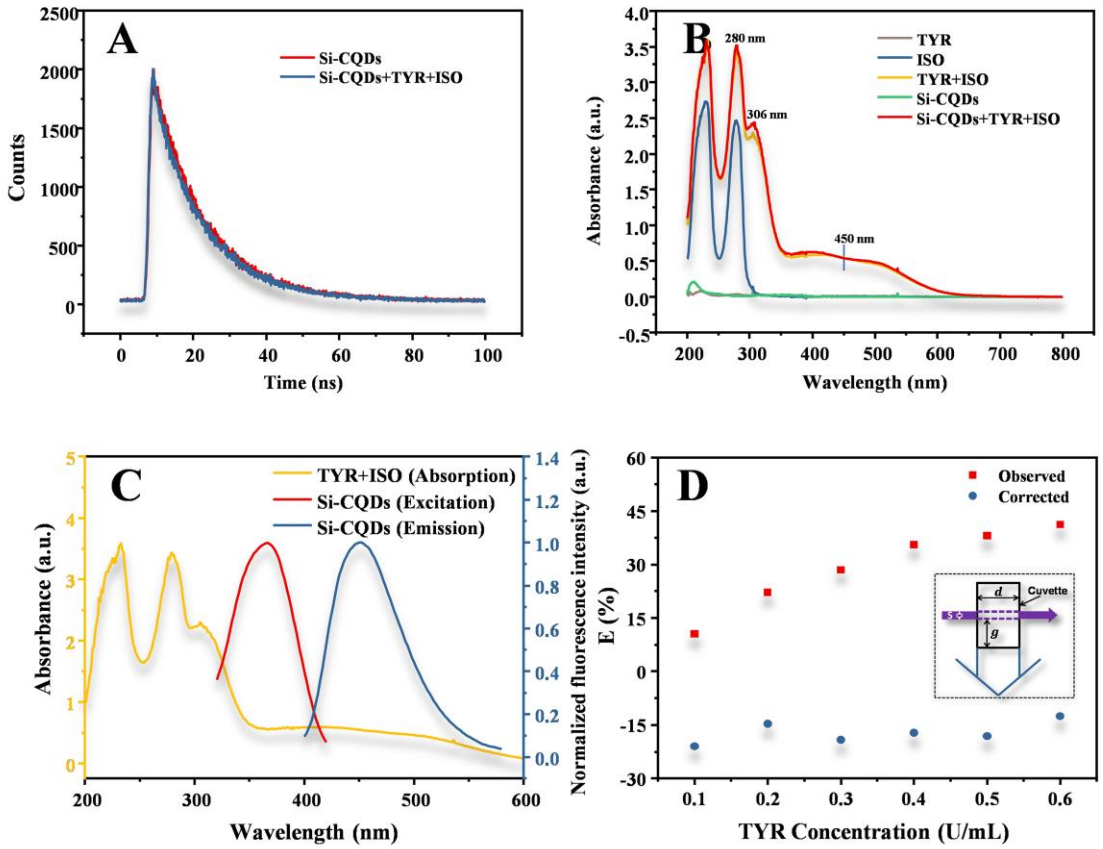

Fig. 3 (A) The fluorescence lifetime decay curves of Si-CQDs without or with TYR+ISO. (B)The UV-vis absorption spectra of TYR, ISO, TYR+ISO, Si-CQDs, Si-CQDs+TYR+ISO. (C) The UV-vis absorption spectrum of TYR+ISO and fluorescence excitation and emission spectrum of Si-CQDs. (D) The detected and corrected inhibition efficiency after IFE is eliminated in Si-CQDs+ISO+TYR with different TYR concentrations. The inset is the parameters used in the Formula S1. The *s* is the thickness of the excitation beam (s=0.10 cm), and the *g* and *d* are the distance and width between the edge of the excitation beam and the edge of the cuvette, respectively (*g*=0.40 cm, *d*=1.00 cm).

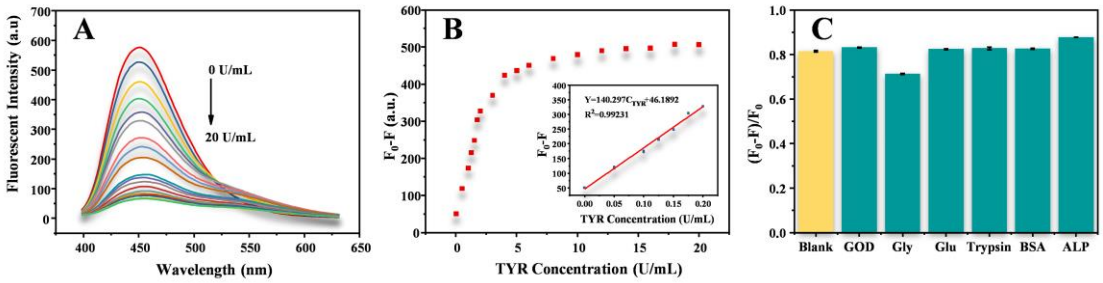

Fig. 4 (A) Fluorescence emission spectra of Si-CDs+ISO with different concentrations of TYR. (B) The concentration and linear relationships (inset in B) between F_0-F and C_{TYR} at different TYR concentrations (0-20 U/mL). (C) The effect of GOD, Gly, Glu, Trypsin, BSA and ALP on the $(F_0\text{-}F)/F_0$ of Si-CQDs+ISO+TYR. The concentrations of GOD, Gly, Glu, Trypsin, BSA and ALP are 5 U/mL, 10 μM, 100 μM, 5 U/mL, 10 μg/mL, and 5 U/mL, respectively.